

# Diffraction Measurements around a Building Corner at 10 GHz

Nuutti Tervo, Claudio Ferreira Dias, Veikko Hovinen, Marko Sonkki,

Antti Roivainen, Juha Meinilä and Matti Latva-aho

Department of Communications Engineering

Centre for Wireless Communications

P.O. Box 4599, FIN-90014 University of Oulu, Finland

{nutervo, cferreir, veikko.hovinen, msonkki, antti.roivainen, jmeinila, matti.latva-aho}@ee.oulu.fi

**Abstract**—This paper presents the results and analysis of diffraction measurements around a building corner at 10 GHz. Radio channel measurement setup contains a 4-port vector network analyzer and two virtual antenna arrays. Angle of arrival analysis is carried out to distinguish the diffracted path from the other multipath components in the impulse response. Results are analyzed with respect to the Fresnel diffraction parameter and diffraction angle, and compared with the knife edge diffraction (KED) and absorbing screen diffraction losses, respectively. The absorbing screen approach is concluded to give reasonable fit for the measurements in the shadow region, but a poor fit near to the shadow boundary and in the illuminated region. The analysis of the corner diffraction shows that a building corner can be modeled by the KED-theory at 10 GHz.

## I. INTRODUCTION

The growth of mobile communication and the advances in technology are leading the world towards fully connected network society. Several research groups around the world are expending huge effort in order to identify the main challenges and key technology components of fifth generation (5G) radio access. In order to fulfill the long-term traffic demands for multi-Gbps data rates, it is necessary to enable very wide transmission bandwidths. Therefore, the future wireless systems need to be able to operate in higher frequencies compared with the frequencies used in the current systems [1].

This paper presents the results and the analysis of diffraction measurements around a building corner at 10 GHz. The authors are not aware of other diffraction measurements at around 10 GHz. However, other channel characteristics and phenomena at this frequency have been investigated and published. For example, at the indoor environment, the channel is observed to be Nakagami-distributed at 10 GHz [2]. An extensive measurement campaign at 11 GHz is presented in [3], where channel characteristics such as path loss, shadowing, delay spread and the coherence bandwidth of the channel are considered. The path loss exponent is stated to be between 2 and 3 in non-line-of-sight (NLOS) indoor environments. Also the path loss is claimed to be almost the same for both the vertical and the horizontal polarizations.

The corner diffraction at 60 GHz is investigated in [4]. The measured diffraction loss is compared with the geometrical theory of diffraction (GTD) and the uniform theory of diffraction (UTD) based diffraction coefficients. The absorbing screen diffraction model is found to give a good fit to the results. The absorbing screen approach ([5, Chap. 5]) is also considered in this paper along the knife-edge diffraction (KED).

In diffraction, only a small change in the antenna position may change the diffraction loss significantly, especially in the region where the direct path and the diffracted path are both present. Virtual antenna array in the transmitter (TX) and the receiver (RX) ends is used enabling us to shift the antennas as only a fraction of wavelength between the recordings. This makes it possible to observe the radio wave behavior in transition from LOS to NLOS channel state. Furthermore, virtual antenna array allows us to employ the angle of arrival (AoA) algorithms to distinguish the diffracted path from the other multipaths. The aspects of the 10 GHz channel highlighted in this work are LOS and NLOS propagations, diffraction loss, and diffraction angle. The results can be applied for the path loss estimation of the diffracted signal path as well as for choosing the valid diffraction models for ray tracing (RT) at 10 GHz.

The rest of the paper is organized as follows. Section II describes the measurement setup and the measurement environment. Section III presents the KED-theory and the absorbing screen approach. Section IV presents the principles of the AoA estimation method applied to detect the diffracted component from the other multipaths. The measurement results are analyzed and compared with the theory in Section V. The suggestions and plans for future activities related to this paper are presented in Section VI and the conclusion is drawn in Section VII.

Notation: Throughout this paper matrices (resp. column vectors) are set in boldface capital (resp. lower case) letters,  $[\cdot]^T$  denotes the transpose and  $[\cdot]^H$  denotes the hermitian transpose of the vector, respectively.

## II. MEASUREMENT SETUP AND ENVIRONMENT

### A. Measurement Equipment

A block diagram of the 10 GHz channel measurement setup is presented in Fig. 1. Rohde & Schwarz ZNB20 4-port vector network analyzer (VNA) [6] was utilized to record the scattering parameters (S-parameters) in the frequency domain. The measurement settings are presented in Table I. The antennas at the TX and the RX were directional dual polarized patch antennas. The antennas have good impedance matching ( $< -13$  dB) and isolation ( $> 24$  dB) between the feeding ports over the measured 500 MHz bandwidth. The antenna layout is presented in Fig. 2a. The radiation patterns (XZ-cut) for the antenna polarizations in terms of total gain at 10.1 GHz are presented in Fig. 2b. VNA ports 1 and 3 were connected to the TX antenna and ports 2 and 4 to the RX antenna, respectively.

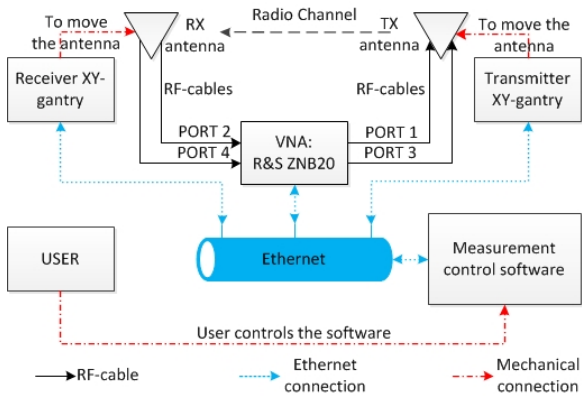


Fig. 1. Block diagram of the radio channel measurement setup.

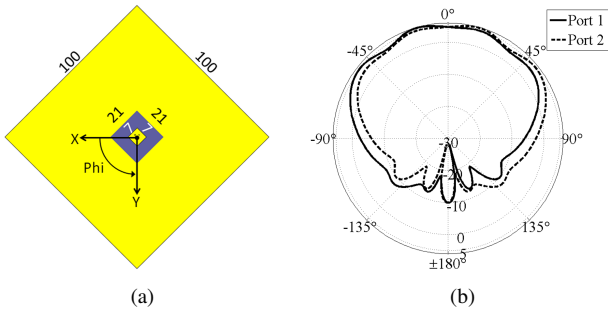


Fig. 2. (a) An overview of the RX/TX antennas and (b) simulated antenna gains of the two orthogonal polarizations at 10.1 GHz (XZ-cut).

TABLE I. VNA SETTINGS

|                      |              |
|----------------------|--------------|
| Frequency range      | 9.85 – 10.35 |
| Transmit power       | 8 dBm        |
| Number of points     | 201          |
| Resolution bandwidth | 10 kHz       |

TABLE II. SPECIFICATIONS OF THE ANTENNAS USED IN THE MEASUREMENTS

|                                   |                     |
|-----------------------------------|---------------------|
| Center frequency                  | 10.1 GHz            |
| -10 dB Bandwidth                  | 720 MHz             |
| Gain                              | > 4 dBi (boresight) |
| Maximum total gain                | 5.8 dBi             |
| Port isolation                    | > 24 dB             |
| Cross polarization discrimination | > 18 dB             |

The antennas were rotated in such a way that the orthogonal polarization planes were tilted at  $\pm 45^\circ$  angle with respect to the vertical. The antenna properties are presented in Table II.

Two vertically positioned XY-gantries were utilized to shift the antennas in the horizontal direction (X-direction) producing virtual planar antenna arrays in TX and RX ends, respectively. MATLAB instrument control toolbox [7] was used to control both the XY-gantries and the VNA.

### B. Measurement Environment

An overview of the measurement environment at the University of Oulu is shown in Fig. 3. The diffracting corner looked from the TX and the RX ends are presented in Figs. 4a and 4b, respectively. The location of the TX virtual antenna array was fixed. The RX was placed in six different locations.

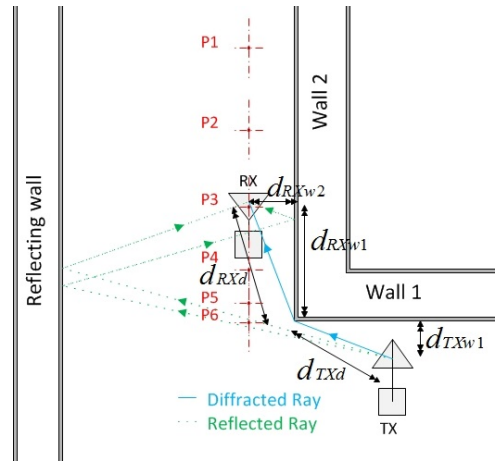


Fig. 3. An overview of the measurement environment.

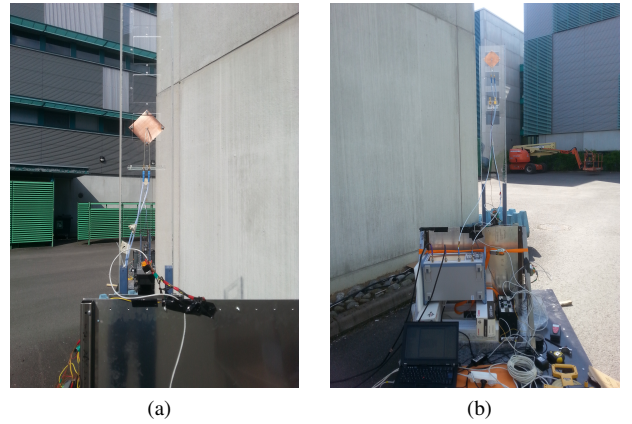


Fig. 4. Diffracting corner looked from (a) TX and (b) RX ends.

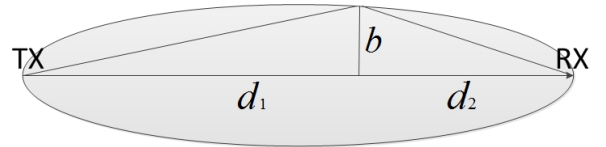


Fig. 5. First Fresnel ellipsoid.

The TX and the RX virtual antenna array configurations were  $10 \times 1$  and  $20 \times 1$ , respectively. The plane of the antenna arrays were perpendicular to the diffracting building corner. The distances to the walls and the building corner were measured in antenna array origins by a laser rangefinder.

### III. PLANE WAVE DIFFRACTION

The radio propagation environment is said to be LOS environment, if the first Fresnel ellipsoid is clear from obstacles [8]. The radius of the first Fresnel ellipsoid can be written as

$$b \approx \sqrt{\frac{\lambda d_1 d_2}{d_1 + d_2}}, \quad (1)$$

where  $\lambda$  is the wavelength and  $d_1$  and  $d_2$  are the distances presented in Fig. 5.

### A. Knife-Edge Diffraction

If there is a sharp, wedge-shaped obstacle inside the first Fresnel ellipsoid, the wave undergoes KED. The diffraction parameter  $\nu$  can be written as [8]

$$\nu = \sqrt{2} \frac{H}{b}, \quad (2)$$

where  $H$  denotes the height of the obstacle with respect to the direct link chord. The KED-coefficient can be expressed as [8]

$$F(\nu) = \frac{1}{2}(1 - (1 - j)(C(\nu) - jS(\nu))), \quad (3)$$

where  $C(\nu)$  and  $S(\nu)$  are Fresnel integrals defined as

$$C(\nu) = \int_0^\nu \cos\left(\frac{\pi}{2}\tau^2\right)d\tau \text{ and } S(\nu) = \int_0^\nu \sin\left(\frac{\pi}{2}\tau^2\right)d\tau, \quad (4)$$

where  $\tau$  is the auxiliary variable for the integral. The diffraction loss factor is the absolute value of the diffraction coefficient. To avoid calculus of complex Fresnel integrals, approximations can be used to calculate the diffraction coefficient for certain  $\nu$ -values. For  $\nu > -0.7$ , the diffraction loss  $L_{ke}$  in dBs can be approximated as [9]

$$L_{ke} = 6.9 + 20 \log(\sqrt{(\nu - 0.1)^2 + 1} + \nu - 0.1). \quad (5)$$

The overall loss of the diffracted signal path is constructed by the free space loss from the TX to the corner, free space loss from the corner to the RX and the loss caused by diffraction. Thus, for the measured total path loss, we can write

$$L_{tot} = L_{fs} + L_{ke} - G_T - G_R, \quad (6)$$

where  $G_T$  and  $G_R$  are the TX and RX antenna gains and  $L_{fs}$  is the free space loss which can be expressed as

$$L_{fs} = 20 \log_{10}\left(\frac{4\pi fd}{c}\right), \quad (7)$$

where  $d$  is the total distance of the path,  $f$  is the frequency and  $c$  is the light speed in free space [8].

### B. Absorbing Screen

Instead of modeling the diffraction by wedges with KED, absorbing screen can also be used to model diffraction. For a plane wave incidence, absorbing screen approach gives us a GTD diffraction coefficient with respect to diffraction angle  $\theta_d$  as [5]

$$D(\theta_d) = \frac{-\sqrt{\lambda}}{2\pi} \left( \frac{1}{\theta_d} - \frac{1}{2\pi - \theta_d} \right), \quad (8)$$

where  $\theta_d$  is the diffraction angle in radians.

## IV. ANGLE OF ARRIVAL

The AoA analysis can be used for estimating the propagation paths of the radio waves from the TX to the RX. In a simple beam scan method for AoA estimation, a steering vector is used in order to scan the signal power over the angular region of interest. The basic equation of the total average output power  $P(\hat{\theta})$  is given by [10]

$$P(\hat{\theta}) = \mathbf{w}^H \hat{\mathbf{R}}_{\mathbf{xx}} \mathbf{w}, \quad (9)$$

where  $\hat{\mathbf{R}}_{\mathbf{xx}}$  is the estimate of the covariance matrix of the multiple-input multiple-output (MIMO) channel and  $\mathbf{w}$  is the array steering vector defined as

$$\mathbf{w} = [1 \ e^{j\mu} \ e^{j2\mu} \ \dots \ e^{j(M-1)\mu}]^T. \quad (10)$$

Here  $M$  is the number of array elements and  $\mu$  is the spatial frequency defined as

$$\mu = \frac{2\pi\Delta}{\lambda} \sin(\hat{\theta}), \quad (11)$$

where  $\frac{2\pi}{\lambda}$  is the wave number,  $\Delta$  is array element spacing and  $\hat{\theta}$  is the estimated AoA.

## V. DATA ANALYSIS AND RESULTS

### A. Combining S-parameters

The diffraction data were recorded by transmitting and receiving two orthogonal linear polarizations. When a linearly polarized wave meets a diffracting knife-edge, the polarization vector is subject to change. To compensate the effect of polarization rotation, we can combine the recorded S-parameters in such a way that the result shows the whole received power. The S-parameters are combined in linear scale as follows

$$A_1 = S_{21} + S_{41} \text{ and } A_3 = S_{23} + S_{43}, \quad (12)$$

where  $A_1$  and  $A_3$  are the recorded channel frequency responses for orthogonal polarizations 1 and 3, corresponding to the VNA TX ports. Here  $S_{21}$  and  $S_{43}$  are the co-polarizations and  $S_{23}$  and  $S_{41}$  are the cross polarizations.

### B. Impulse Response Analysis

The conversion from frequency domain to the time domain is done via 201-point Inverse Discrete Fourier Transform (IDFT). Let us denote  $S_{lm}(f_n)$  as the frequency domain S-parameters, where  $l$  and  $m$  are the port indices and  $f_n$  is the  $n$ th recorded frequency sample. By IDFT, impulse responses  $h_{lm}$  can be written as

$$h_{lm}(t_n) = \frac{1}{N} \sum_{k=0}^{N-1} S_{lm}(f_k) e^{i2\pi kn/N}, \quad (13)$$

where  $t_n$  is the  $n$ th time instant and  $N$  is the number of frequency points [11]. In order to prevent the frequency leakage, hamming filtering was used for the impulse responses. The properties of the calculated impulse responses are given in Table III.

TABLE III. PROPERTIES OF THE CALCULATED IMPULSE RESPONSES

|                                |        |
|--------------------------------|--------|
| Number of samples              | 201    |
| Delay resolution               | 2 ns   |
| Unaliased length (time)        | 400 ns |
| Path resolution                | 60 cm  |
| Maximum detectable path length | 120 m  |

In the measurement environment, the propagating wave undergoes also other multipath propagation phenomena besides diffraction. For example, the wall seen on the left in the Fig. 3, causes reflection. Also, there is a double reflection by the reflecting wall and the wall 2. Thus, the reflected components are seen in the impulse response as well as in the AoA plot in some antenna locations. The sample of the recorded impulse response in the measurement point 4 is depicted in Fig. 6. The reflected and the diffracted multipath components are marked out in the figure.

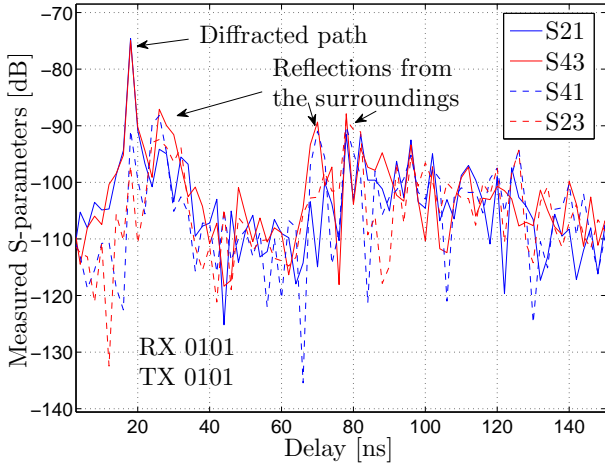


Fig. 6. Sample of the recorded impulse response.

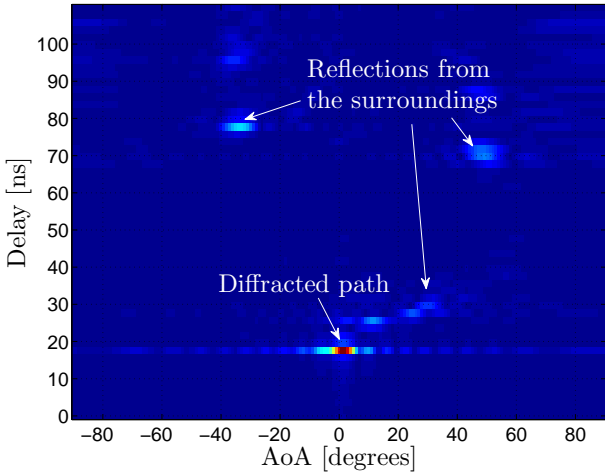


Fig. 7. Azimuth AoA estimated by the beam scan method.

To distinguish the diffracted components from others, we considered two methods. We can roughly assume that the first arriving multipath component is the diffracted one. However, especially in the measurement points 5 and 6, we have also LOS-component affecting to the results. We can estimate the time delay from the measured physical distances, and use this information to time gate the impulse responses. By looking up the components received within some time window around the estimated propagation delay, we can pick up the diffracted one. Using the AoA algorithms, we can estimate the azimuth AoA and thus ensure that the chosen component is the diffracted one. A sample figure of the AoA estimated for the measurement point 4 by the beam scan method (9) is presented in Fig. 7. Both of the described methods were used to detect the diffracted component from the others.

### C. Free Space Loss Cancellation

Instead of keeping the distance to the wall 2 in Fig. 3 as a constant, we measured it separately in each receiver position. The actual positions of the antenna elements with respect to the diffracting corner as an origin are presented in Fig. 8. The

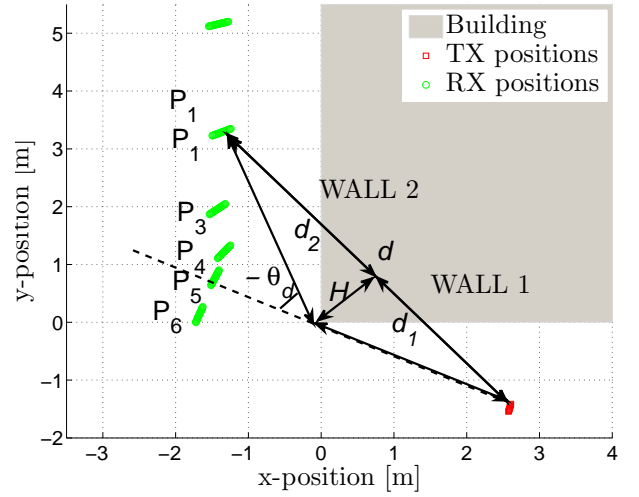


Fig. 8. Antenna locations with respect to the diffracting corner.

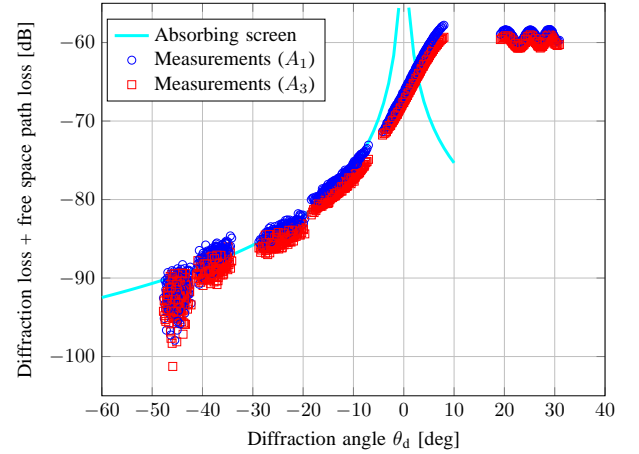


Fig. 9. Diffraction loss as a function of diffraction angle  $\theta_d$ .

precise antenna positions were calculated by trigonometry, knowing that the antenna spacing of the virtual planar array is half of the wavelength and the facing is towards the corner, respectively. The Fresnel ellipsoid is calculated for each TX-RX antenna pair separately by (1). By the measured distances and calculated Fresnel ellipsoids, diffraction parameters  $\nu_i$  were calculated individually for each channel.

In each measured channel, the radio wave travels slightly different distances in the free space. To identify the effect of diffraction from the results, we have to cancel out the free space loss differences between the different points in the results. This was done by bringing all the antenna locations within to the same reference distance from the diffracting corner such that the diffraction angle does not change. The free space loss from the real measured antenna locations to the reference distance points are cancelled out from each measured channel individually.

### D. Diffraction Loss

The measured diffraction losses as a function of diffraction angle and the diffraction loss calculated by absorbing screen approximation (8) are presented in Fig. 9. An offset of  $-59.5$

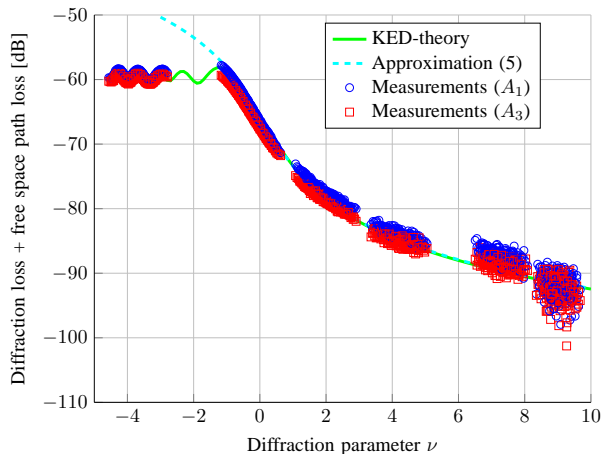


Fig. 10. Diffraction loss as a function of diffraction parameter  $\nu$ .

dB caused by the free space loss and the measurement equipment is added to the theoretical diffraction loss. As we can see from Fig. 9, the absorbing screen approach fits to the measurements only in the shadow region when  $\theta_d < -10^\circ$ . In the illuminated region, i.e when  $\theta_d \geq 0^\circ$ , the absorbing screen approach differs significantly from the measurements.

The measured diffraction losses as a function of diffraction parameter  $\nu$  are presented in Fig. 10. The theoretical KED loss given in (3) and the approximation (5) are presented in the same figure with the  $-59.5$  dB offset. The data measured by the two TX polarizations follows the same graph, but with slightly different offset parameters. The offset difference in two orthogonal polarizations ( $\pm 45^\circ$ ) is estimated to be caused by the antennas and the polarization dependent wave behavior at the diffracting edge. According to the measurements, the difference is approximately 2 dB.

From the Fig. 10, it can be seen that the diffraction loss follows the KED-theory with a good precision. Even in the region where  $\nu \leq -0.7$ , the KED-theory and the measured data are close to each other. Thus, the single KED-loss can be used for calculating the path loss for the diffracted wave propagating behind the building corner at 10 GHz. Furthermore, approximation presented in (5) can be used to calculate the diffraction loss when  $\nu > -0.7$  and Fresnel integrals presented in (4) are not needed to be calculated in the shadow region. According to the measurements, it can be concluded that the diffraction loss is better to be calculated with respect to the KED-parameter  $\nu$ , because it describes better the geometry of the environment than the diffraction angle at 10 GHz. The KED-theory gives the better fit to the results than the absorbing screen approach.

## VI. FUTURE WORK

In this work, we have observed the KED-theory from a point-of-view which does not separate the effect diffraction for two orthogonal linearly polarized waves. To extend the observations of the results, UTD can be used to calculate the diffraction coefficients for both vertical and horizontal polarizations. The measurement setup will also be applied to other measurement scenarios at 10 GHz. Furthermore, virtual planar antenna arrays will be used to measure MIMO channels with large antenna configurations in static environments.

## VII. CONCLUSION

In this paper, the results and analysis of the diffraction measurements around a building corner at 10 GHz were presented. Radio channel measurement setup containing 4-port VNA and two virtual antenna arrays was used to produce high precision antenna movement with respect to the diffracting corner. AoA analysis was carried out to distinguish the diffracted paths from the other components seen in the impulse response. Results were analyzed with respect to the Fresnel diffraction parameter and diffraction angle, and compared with the KED and absorbing screen diffraction losses, respectively. The absorbing screen approach was concluded to give reasonable fit for the measurements in the shadow region, but a poor fit in near to the shadow boundary and in the illuminated region. Analysis of the corner diffraction showed that a building corner can be modeled by the KED-theory at 10 GHz and the simple KED-approximation is valid. Thus, approximation (5) can be used to calculate the diffraction loss and the Fresnel integrals do not have to be calculated in the shadow region, when considering the diffraction around the building corner at 10 GHz. Furthermore, KED can be used as a diffraction loss model for RT at 10 GHz.

## ACKNOWLEDGMENT

This work has been supported by Broadcom Communications Finland Oy, Elektrobit Wireless Communications Oy, Huawei Technologies Oy (Finland) Co. Ltd, Nokia Networks Oy and Finnish Funding Agency for Innovation (Tekes).

## REFERENCES

- [1] E. Dalman, G. Mildh, S. Parkwall, J. Peisa, J. Sachs, and Y. Selén, "Ericsson Review 6/2014. 5G radio access," Tech. Rep., 2014.
- [2] A. Abouraddy and S. Elnoubi, "Statistical modeling of the indoor radio channel at 10 GHz through propagation measurements .I. Narrow-band measurements and modeling," *IEEE Transactions on Vehicular Technology*, vol. 49, no. 5, pp. 1491–1507, Sep 2000.
- [3] M. Kim, Y. Konishi, Y. Chang, and J.-I. Takada, "Large Scale Parameters and Double-Directional Characterization of Indoor Wideband Radio Multipath Channels at 11 GHz," *IEEE Transactions on Antennas and Propagation*, vol. 62, no. 1, pp. 430–441, Jan 2014.
- [4] J. Lu, P. Cabrol, D. Steinbach, and R. Pragada, "Measurement and Characterization of Various Outdoor 60 GHz Diffracted and Scattered Paths," in *IEEE Military Communications Conference, MILCOM*, Nov 2013, pp. 1238–1243.
- [5] H. L. Bertoni, *Radio Propagation for Modern Wireless Systems*. Prentice Hall PTR, 2000.
- [6] Rohde & Schwarz ZNB Vector Network Analyzer: User Manual, (Accessed 10.9.2014). [Online]. Available: [http://cdn.rohde-schwarz.com/pws/dl\\_downloads/dl\\_common\\_library/dl\\_manuals/gb\\_1/z/znb\\_1/ZNB\\_ZNBT\\_UserManual\\_en\\_25.pdf](http://cdn.rohde-schwarz.com/pws/dl_downloads/dl_common_library/dl_manuals/gb_1/z/znb_1/ZNB_ZNBT_UserManual_en_25.pdf)
- [7] *MATLAB Instrument Control Toolbox; Users Guide*, (Accessed 25.8.2014). [Online]. Available: <http://www.mathworks.se/help/instrument/index.html>
- [8] S. Saunders and A. Aragón-Zavala, *Antennas and Propagation for Wireless Communication Systems: 2nd Edition*. John Wiley & Sons, 2007.
- [9] ITU-R Recommendation P.526-7: Propagation by diffraction. [Online]. Available: [https://www.itu.int/dms\\_pubrec/itu-r/rec/p/R-REC-P.526-7-200102-S!!PDF-E.pdf](https://www.itu.int/dms_pubrec/itu-r/rec/p/R-REC-P.526-7-200102-S!!PDF-E.pdf)
- [10] Z. Chen, G. Gokeda, and Y. Yu, *Introduction to Direction-of-arrival Estimation*. Artech House, 2010.
- [11] D. Sundararajan, *The Discrete Fourier Transform: Theory, Algorithms and Applications*. World Scientific Publishing Company, Incorporated, 2001.